CHAPTER 8

Seasonal Variations of Polygonal Thermal Contraction Crack Patterns in a South Polar Trough, Mars

Abstract

We present observations of seasonal variations in polygonal crack patterns located in a polar trough on the south polar cap of Mars; previously, there was no direct observation showing that these patterns change. Polygonal patterns on Mars are attributed to thermal contraction cracking, which is commonly observed in periglacial environments on Earth. In this paper we discuss observations based upon the high-resolution image data of the Mars Orbiter Camera (MOC) and focus on the reconstruction of their seasonal development. The image-based observations are further supported by temperature data obtained by the Thermal Emission and Imaging Spectrometer (THEMIS) and the Thermal Emission Spectrometer (TES) instruments. We show that the south polar trough pattern is located in an active geologic unit, which undergoes seasonal variations and annual crack formation. Furthermore, there are strong indications showing these contraction-crack processes take place in a thin layer that might be composed of water-ice and is located beneath the seasonal carbon-dioxide ice cover.

8.1. Introduction

As part of our mapping and classification work focused on Martian south polar polygonal patterns (*van Gasselt et al.*, 2003b; *van Gasselt et al.*, 2004), we have taken special interest in areas that have been imaged two or more times by the Mars Orbiter Camera (MOC) instrument onboard Mars Global Surveyor (MGS) in order to identify seasonal variations and surface modifications.

In this paper we present multi-temporal observations of variations in polygonal patterns and a qualitative discussion regarding their formation on the basis of several high-resolution MOC Narrow Angle (MOC-NA) images that cover a south polar trough (SPT) at about 281° eastern longitude and 87° southern latitude (figure 8.1). This SPT is incised into the south polar residual cap, exposing underlying dark-lane deposits.

Our discussion is predominantly based upon image observations at two locations and is further supported by surface temperature data obtained by the Thermal Emission Spectrometer (TES) onboard MGS and the brightness temperature record obtained through the Thermal Emission Imaging Subsystem (THEMIS) onboard Mars Odyssey (MO). As the observed polygonal pattern is situated in a polar trough, where desiccation or contraction cracking due to lava cooling

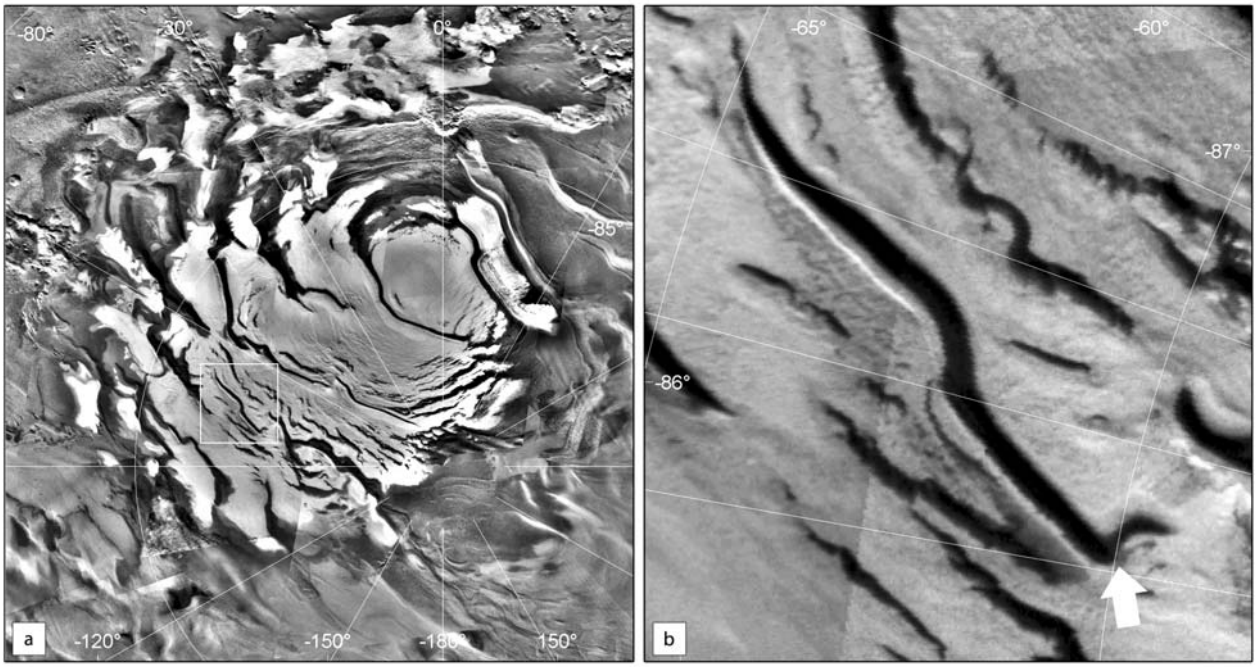

Figure 8.1.: Overview map of the south polar cap and the study area. [a] stereographc projection of the residual south polar cap (MDIM-2.1), box refers to location of scene [b]; [b] south polar trough and study area located between 86°S to 87°S and 275°E to 300°E. White arrow points towards trough location and the MOC-NA based observations; the observed area lies within a polar trough (dark lane) which is incised into the residual south polar cap; this scene is a summer-time image of that area showing the dark, CO_2-ice free interior of the polar trough; image maps are based upon the Viking Orbiter Mars Digital Image Mosaic MDIM 2.1, released in 2004.

do not occur, we will hereafter discuss our observation in the context of thermal contraction cracking of the surface caused by large seasonal temperature gradients.

8.2. Background

Small-scale polygonal patterns are characteristic landforms familiar to both periglacial and desert environments on Earth. Their formation is attributed either to thermal contraction cracking of the surface layer (frost fissures) or to desiccation of mud sediments, respectively. After almost two centuries of terrestrial investigations (*Figurin* (1823) in *Washburn* (1979a)), theoretical modeling (*Leffingwell*, 1915; *Lachenbruch*, 1962) and detailed field work (*Black*, 1974; *Mackay*, 1974; *MacKay*, 1975, 1986; *Mackay*, 1992), the mechanisms involved in thermal-contraction cracking processes are reasonably understood although the results of theoretical models often are not supported by evidence from field work (*French*, 1996; *Lachenbruch*, 1962; *Black*, 1976; *Mackay*, 1992).

In general, polygonal crack patterns occur in terrestrial permafrost when a rapid temperature drop causes a contraction of the permafrost material which is controlled by the coefficient of linear expansion of ice (*Leffingwell*, 1915; *Lachenbruch*, 1962; *French*, 1996). The initial fissures and cracks might close during spring seasons or, if seasonal thaw water is present, might be filled with water, which freezes during colder periods and produces a vertical ice vein. An initial fissure presents a mechanically weak zone in the strength of permafrost, therefore it is probable that an ice-filled fissure will be re-opened during the next freeze cycle and new thaw water will penetrate. After several years of freeze-thaw cycles, a ver-

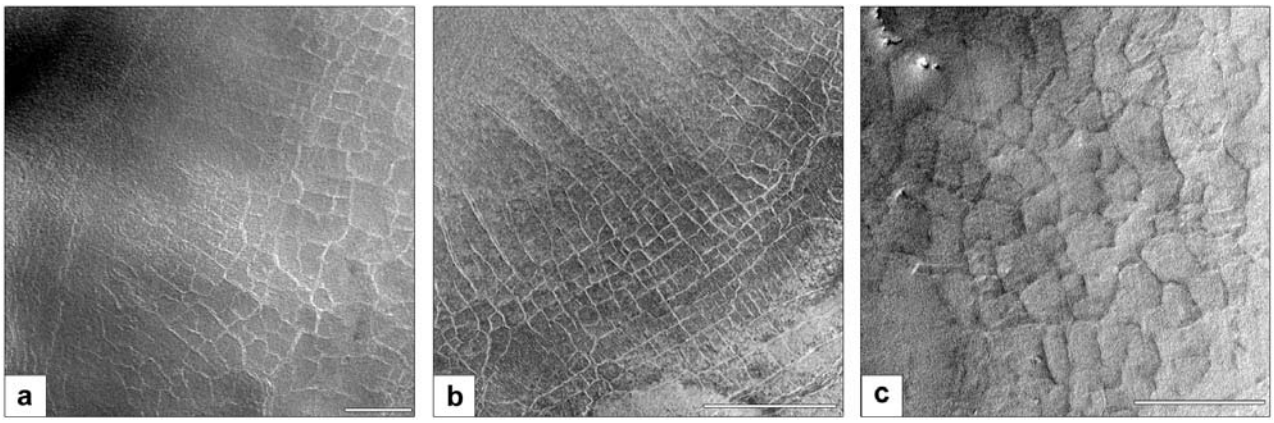

Figure 8.2.: Examples of characteristic polygonal terrain located in the Martian mid-latitudes, images were taken by the MOC-NA instrument during its primary mapping phase. (a) MOC-NA M03/00350, (b) MOC-NA M08/06179, (c) MOC-NA M09/04950. The oriented orthogonal polygonal pattern in (a) and (b) occurs frequently on crater slopes and resemble terrestrial periglacial polygons caused by thermal contraction cracking of the upper surface layer. The outer rims of such cracks are often slightly upturned and form a central trench under which a vertical ice- or sand-wedge might be situated. The scale bar is 500 meters in each scene, North is at top, map projection is sinusoidal.

tical ice wedge might form and can reach a depth of up to several tens of meters and exceed a surface width of four meters (*French*, 1996). In plan view, the fissures propagate over several tens of meters, intersect at characteristic angles and form orthogonal or hexagonal polygonal shapes. In environmental conditions where moisture is not available, sand might instead penetrate into the fissures and produce vertical sand-wedges as described by *Péwé* (1959).

Martian landforms with a striking resemblance to terrestrial periglacial polygonal systems (figure 8.2) have been observed and characterized for the first time on the basis of Viking Lander images and high-resolution Viking Orbiter frames (*Mutch et al.*, 1977; *Lucchitta*, 1981; *Lucchitta*, 1983). These Martian mid-latitude landforms have been interpreted as possible ice-wedge polygons (*Mutch et al.*, 1977; *Lucchitta*, 1981). It has to be kept in mind, however, that ice-wedges as an expression of vertical and lateral growth of ice-filled contraction fissures require seasonally liquid water. New insights regarding the origin and especially the global distribution of polygonal crack networks have been provided by several authors on the basis of high-resolution data from the MGS MOC-NA instrument (*Malin et al.*, 1992; *Malin and Edgett*, 2001). Research concentrates on comparative morphologic and morphometric issues (*Yoshikawa*, 2000; *Seibert and Kargel*, 2001; *Kuzmin et al.*, 2002; *van Gasselt et al.*, 2003b; *Mangold et al.*, 2004), resurfacing times (*Sletten et al.*, 2003) and the global as well as regional distribution (*Kuzmin and Zabalueva*, 2003; *van Gasselt et al.*, 2003b). In-depth models on the formation linked to the theory of *Lachenbruch* (1962) have been provided by *Mellon* (1997).

The characteristic small-scale landforms have been identified in mid-latitudes between 38° and 70° north and south (*Seibert and Kargel*, 2001; *Kuzmin and Zabalueva*, 2003; *Mangold et al.*, 2004) as well as in the south polar area (*Kossacki and Markiewicz*, 2002; *Piqueux et al.*, 2003; *van Gasselt et al.*, 2003b). The two-belt distribution in mid-latitudes generally corresponds with the distribution of various permafrost related morphologies (*Squyres*, 1978, 1979; *Squyres and Carr*, 1986; *Squyres et al.*, 1993) and theoretical models of depths of permafrost (*Zent et al.*, 1986; *Paige*, 1992; *Mellon*, 1997). The diameters of Martian polygonal features, which range from a few meters to several hundred meters (*Seibert and Kargel*, 2001; *Yoshikawa*, 2000; *Kuzmin et al.*, 2002; *van Gasselt et al.*, 2003b), are very similar to their terrestrial

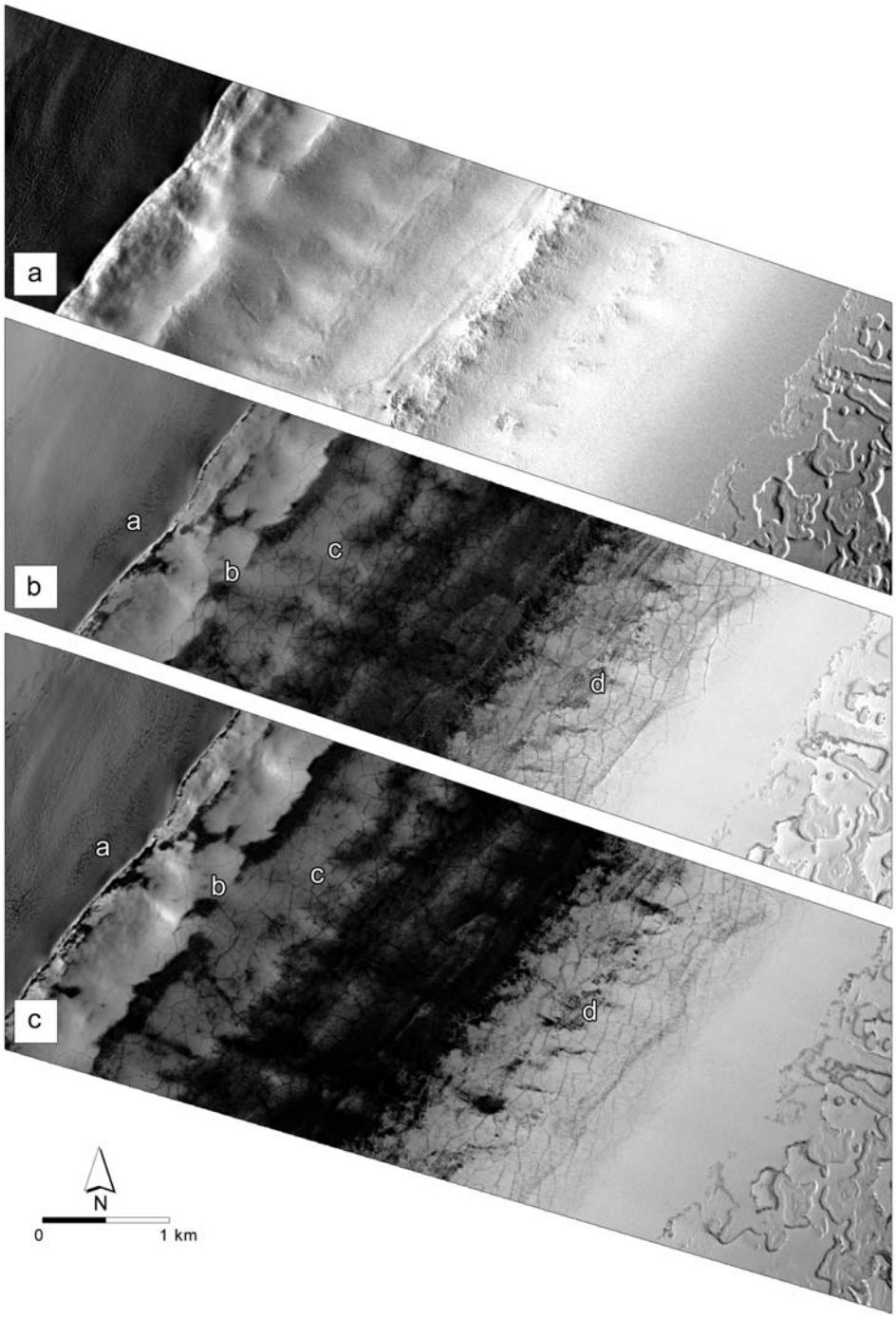

Figure 8.3.: Three overlapping MOC-NA image scenes at location A crossing a south polar trough which is incised into the residual cap at 281.4°E and 87.0°S. (a) MOC-NA M07/02129 was acquired in mid-September 1999 at L_S = 204.1° with a scaled pixel width of 1.38 meters. (b) MOC-NA M12/00730 was taken in February 2000 at L_S = 296.7° with a scaled pixel width of 1.38 meters. (c) MOC-NA E11/03905 was acquired in late December 2001 at L_S = 297.6° with a scaled pixel width of 1.45 meters. Lower-case letters in (b) and (c) refer to image scenes in figure 8.11. Also note, that within the 'swiss-cheese' terrain slight enlargements of intra-mesa pits can be observed in the summer-time image data, as described in detail by e.g., *Thomas et al.* (2000); *Malin and Edgett* (2001); *Byrne and Ingersoll* (2003). The images have been processed and stereographically projected with a center longitude of 281.4°E and a map scale of 1.70 meters per pixel. Sun illumination comes from the west in all three images.

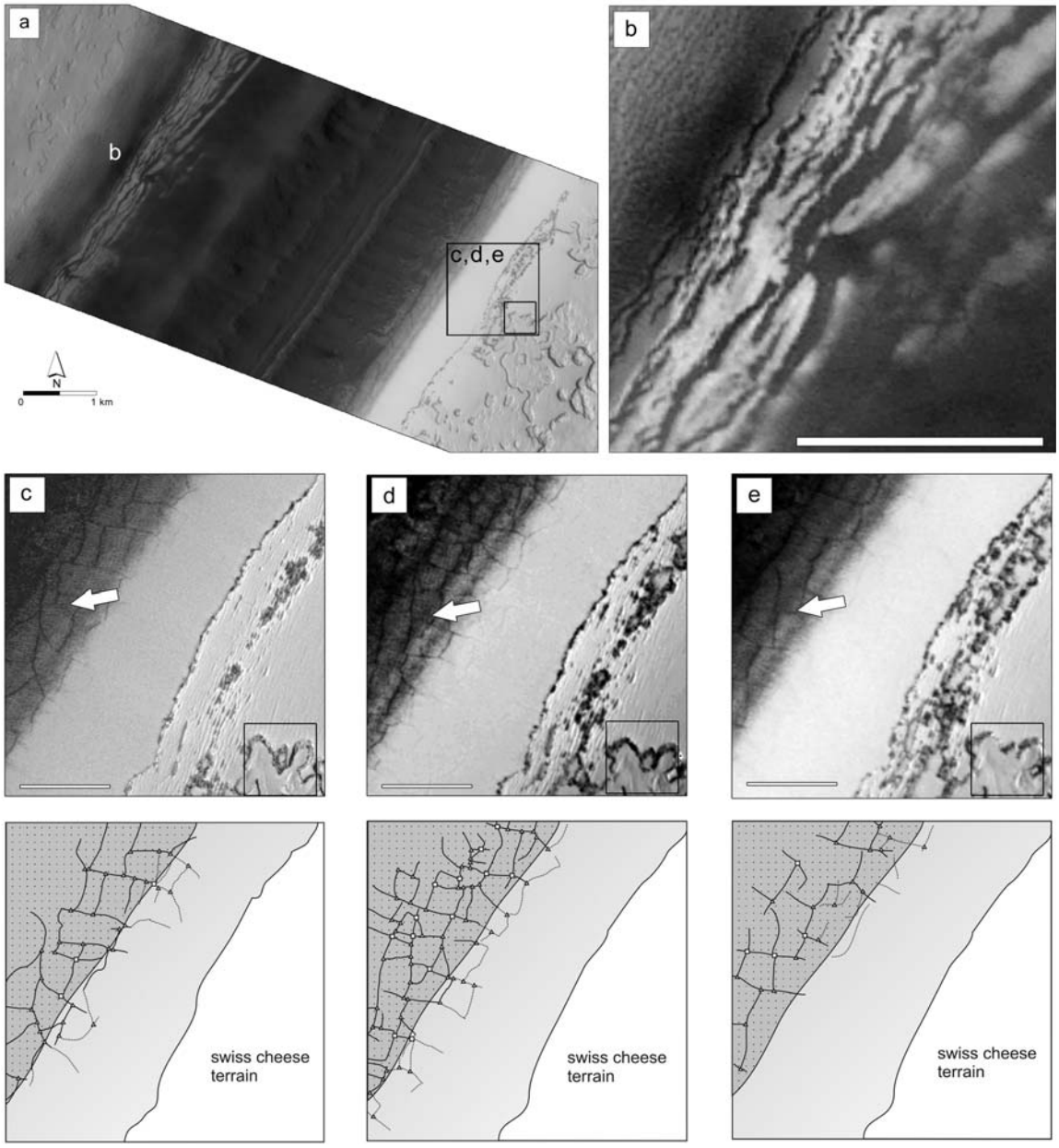

Figure 8.4.: Composition of MOC-image examples for location B located to the southeast of location A. (a) MOC-NA R11/04160 shows a traverse of the same SPT in summer, when seasonal CO_2 has sublimated completely. The southeastern rim belongs to the residual polar cap and shows the characteristic 'swiss-cheese' terrain. At the transition between rim and trough-center several polygon patterns can be observed which are re-generated each year (c-e). (b) shows the trough-parallel configuration of seasonal CO_2 and dark material. Scale bar is 500 meters. Image sequence (c) M12/02337, (d) E12/00629, and (e) R11/04160 show repeated MOC images with scenes from the southeastern trough in (a). All images were obtained during mid-summer (L_S = 304°–306°). In images c-e a different polygonal pattern is visible as illustrated by the sketch map below each image. Furthermore, it is noteworthy that the 'swiss-cheese' terrain pattern (lower right-hand quadrangle) has been altered.

counterparts (*Lachenbruch*, 1962, 1966; *Black*, 1976; *French*, 1996; *Yershov*, 2004).

While definitive evidence for the method of formation of small-scale polygons is lacking, image interpretation combined with studies on ice stability in the Martian regolith and measurements by the Neutron Spectrometer instrument onboard MO (*Mangold et al.*, 2004) suggests that these landforms are the result of thermal contraction cracking of the upper surface layer.

In contrast to the mid- and high-latitude polygonal patterns, the Martian south polar region (figure 8.3 and 8.4) is being currently investigated with the primary focus on the distribution, type classification and correlation with geologic units (*van Gasselt et al.*, 2003b). Only a few results regarding correlation with the distribution and influence of subsurface water have been presented (*Kossacki and Markiewicz*, 2002; *Piqueux et al.*, 2003). It seems, however, that variations in the structure and dimensions of polygonal landforms are greater in the south polar region when compared to the mid- and high-latitude regions.

In contrast to the north polar cap where residual ice consists of water (*Kieffer et al.*, 1976) with small admixtures of dust, the south polar residual ice consists predominantly of carbon dioxide (*Kieffer*, 1979).

It has been suggested that the south polar cap contains a considerable water reservoir beneath the perennial carbon dioxide cover (*Jakosky and Barker*, 1984). The detection of substantial amounts of buried hydrogen (*Boynton et al.*, 2002) and theoretical models (*Titus et al.*, 2003) have been finally confirmed after direct measurements by the OMEGA spectrometer onboard Mars Express (*Bibring et al.*, 2004) showed that considerable amounts of water reside below the residual carbon dioxide cap and in areas adjacent to it. The composition and thermal environment of the south polar layered deposits (SPLD) underneath the residual ice cap seems to provide an ideal environment for the formation of contraction crack polygons.

8.3. Data Source and Processing

8.3.1. MOC Image Data

In order to estimate the accuracy of the data and the validity of observations, we briefly describe the main procedures concerning the image data preparation. For photogeologic interpretation and measurement purposes, all MOC-NA compressed raw images have been processed using standard USGS ISIS and JPL VICAR routines. For location A (figure 8.5), the processed image data have a horizontal resolution between 1.43 meters per pixel (M12/00730), 1.84 meters per pixel (E11/03905) and 2.18 meters per pixel (M07/02129). In order to achieve maximum accuracy and comparability, the image data have been (a) pre-rectified using the MOLA digital terrain model and (b) projected stereographically with a map scale of 1.70 meters per pixel, a center longitude of 281.4°E and a center latitude of 90°S. The accuracy of the MOC-NA camera pointing ensured that offsets were less than six to seven pixels in each direction. Artifacts due to different imaging parameters can be ruled out for following reasons: The local true solar times during imaging are between 18.13 (M12/00730), 18.32 (E11/03905) and 19.39 decimal hours (M07/02129). This results in rather high but almost identical incidence angles of 68° for both M12/00730 and E11/03905 as well as 81° for M07/02129. MOC-NA images M12/00730 and E11/03905, which have been prepared for a statistical comparison, have time offsets of only 0.19 decimal hours and variations in incidence-angles are negligible. The large emission-angle difference of approximately 18° between M12/00730 and E11/03905 has no influence on the image geometry after orthorectification using the digital terrain model. For mapping purposes and comparability of polygon statistics, minor corrections using manual tie point selections and image rectification have been performed. The accuracy of camera pointing and nearly identical imaging parameters make the overall image-comparability of the images at location A outstanding (s. Table 8.1). The map scales of MOC-NA scenes for location B (fig-

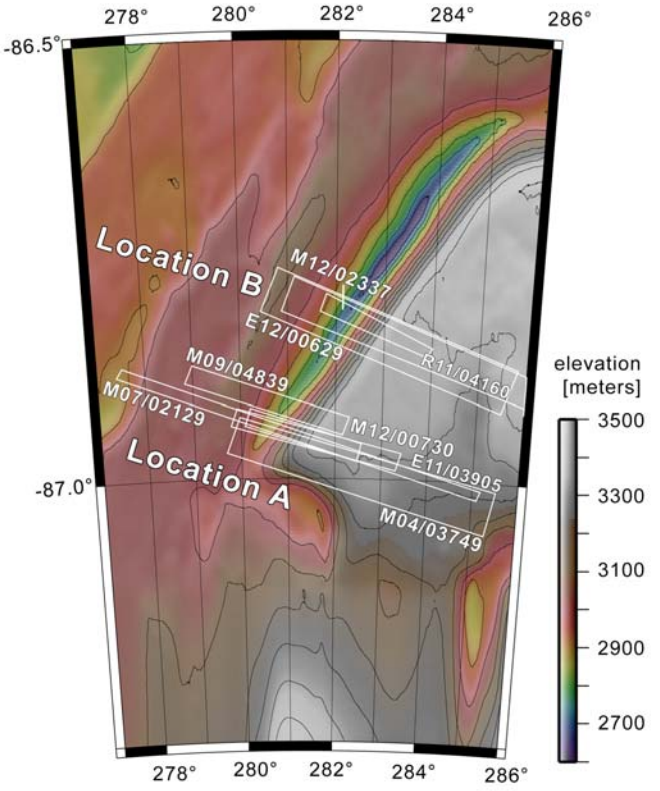

Figure 8.5: Mars Orbiter Laser Altimeter derived topographic map of the south polar trough (SPT) and contour lines with an interval of 50 meters. White boxes show the MOC-NA image footprints for location A and B as described in the main text. Map projection is stereographic, North is at top.

ure 8.5) range from 1.4 meters per pixel (M12/02337) to 2.9 meters per pixel (E12/00629, R11/04160). The center longitude for all images is 283.3°E. As these scenes were not utilized for mapping purposes and statistics, no manual rectification has been applied. The imaging parameters for location B are equal to location A (s. Table 2).

8.3.2. THEMIS and TES Data

Calibrated temperature data from the TES-instrument onboard MGS have been collected using the provided Vanilla software package. In order to characterize the surface of the polar trough throughout the Martian south polar seasons, we collected data during MOC-image acquisition for location A (i.e., $L_S = 204° \pm 3°$ and $L_S = 297° \pm 3°$). To obtain a representative data set, the data lists have been split into day-time (10h-16h) and night-time (20h-6h) values (figure 8.6). Surface pressure data have been excluded as they showed nearly constant values throughout the seasons and are below 4 mbar, allowing sublimation of CO_2 at approximately 140 K.

The ground resolution of the TES data varies with the flight altitude of the MGS spacecraft. The instantaneous field of view (IFOV) is 8.5 mrad (*Christensen et al.*, 2001), which provides a 2800 to 3000 meter pixel resolution for the TES measurements at an altitude of 350 km. In order to account for multiple orbit coverage, data have been median filtered and plotted with the appropriate pixel sizes. For direct comparison with the MOLA topography (IAU2000), TES data (IAU94) have been adjusted to fit the MOLA reference (i.e., planetocentric latitudes, positive easting). As the spatial resolution of the TES data is not high enough to resolve the polar trough in detail, MOLA contour lines have been overlaid in each TES plot. We are aware that a ground surface sampling interval of approximately 3 km, which in fact covers the major parts of the trough, will obscure the data and present only approximated values. Moreover, the data have natural limitations (e.g., noise ratios, calibration errors, atmospheric effects, errors in the low-temperature regime) (*Christensen et al.*, 1992, 2001).

Mid-winter data are not available due to the mapping

Table 8.1.: Original MOC-NA image characteristics of M07/02129, M12/00730 and E11/03905 at location A (281.4°E). The individual scenes cover the southwestern part of the SPT. The summer-time images have been analysed for the characterization of the polygonal pattern. MOC-NA image characteristics of M12/02337, E12/00629 and R11/04160 are for location B (283°E), covering the central part of the SPT.

MOC-NA		M07/02129	M12/00730	E11/03905
true solar time	[dec. h.]	19.39	18.13	18.32
imaging date	[dd-mm-yyyy]	11-09-1999	06-02-2000	26-12-2001
pixel width	[m/px]	2.18	1.43	1.84
solar longitude	[°]	204	297	297
center longitude	[°E]	281.4	281.4	281.7
incidence angle	[°]	80.9	67.8	68.1
emission angle	[°]	0.3	0.3	17.9
north azimuth	[°]	161	162	164
sun azimuth	[°]	59	68	68
MOC-NA		M12/02337	E12/00629	R11/04160
true solar time	[dec. h.]	17.68	17.89	18.16
imaging date	[dd-mm-yyyy]	23-02-2000	06-01-2002	28-11-2003
pixel width	[m/px]	1.38	2.90	2.90
solar longitude	[°]	306.5	304.4	306.4
center longitude	[°E]	282.8	283.1	283.7
incidence angle	[°]	69.8	69.4	70.1
emission angle	[°]	0.3	17.9	17.9
north azimuth	[°]	156	159	160
sun azimuth	[°]	70	69	66

characteristics of the TES instrument, while mid-spring data, taken at L_S=225° ± 3° and failing to cover the SPT, have therefore been excluded. Fortunately, several TES measurements cover the SPT very well during relevant dates, making a reconstruction partly possible.

In order to estimate the accuracy of the TES data measurements, we additionally utilized a high-resolution THEMIS brightness temperature record (BTR) and compared the brightness temperature values for both instruments (figure 8.7 and 8.6d-f). Without knowing the surface emissivity, the brightness temperature of course provides no information about the real surface temperatures. We can clearly see that brightness temperature during L_S = 313° drops from > 225 K at the center of the trough to about 165 K at its outer rim. This 60 K-temperature decrease over a lateral distance of about three to four kilometers would be incorporated into a single brightness temperature value within the TES data. As a result, we would expect a true value between these two extremes, depending on where TES took its measurements. Therefore, it is reasonable to assume slightly larger values for the trough interior than those acquired by TES.

8.4. Observations

In this paper we focus on two locations, referred to as location A and location B (figure 8.5), in order to provide insight into the seasonal development of the SPT located at about 281.0° E and 87.0° S. Location A has been imaged at least five times between 1999 and

2001.
Three images were acquired with a considerable overlap (M07/02129, M12/00730 and E11/03905). MOC-NA image M04/03749 has been excluded from our discussion as it is nearly identical to the M07/02129 scene. Image M09/04839 does not show a significant overlap with the other three images but has been included so that the analysis of seasonal variations can be completed. Location B is located near the center of the SPT and is covered by three MOC scenes (M12/02337, E12/00629 and R11/04160), which were all taken during the summer-seasons in 2000, 2002 and 2003. In contrast to the images for location A, these images have a more supplementary character and were processed using standard processing methods. See figure 8.8 for a diagram showing the timeline of MOC-image acquisition.

8.4.1. Topographic and Morphologic Settings

The SPT is one of several circum-polar spiraling troughs that cut into the residual polar ice cap, revealing dark-lane material beneath.
The rims of the northeast-southwest trending SPT and their adjacent terrain have a mean topographic elevation of approximately 3200 meters in the southeast and 3000 meters in the northwest (figure 8.5). At its center, the elevation of the trough is approximately 2700 meters to 2800 meters. In the southwest, the trough becomes more narrow and shallow and bends to the southeast, where it terminates as a conical hook-shaped depression. The trough is characterized by several large rim-parallel ridges and furrows, which are irregularly shaped and form a highly undulated terrain surface.
In cross-section, the trough is highly asymmetrical (figure 8.9) with a southeastern (sunlit) flank that is steeper in its upper part and reaches and elevation of 3170 meters (over MOLA reference datum). The lower region of the flank slopes more gently towards the center of the trough, which is located at an elevation of approximately 2820 meters. The overall slope angle is approximately 4° to 5°. The northwestern flank slopes gently (about 3°) to an elevation of approximately 3000 meters.
In the image data for location A (figure 8.3), the SPT has a maximum width of about 7 km and is framed by a smooth, relatively dark deposit on the northwestern trough shoulder and a well defined so-called 'swiss-cheese' pattern on the southeastern flank. The darker deposit on the northwestern flank extends to the border of the MOC-NA image M07/02129 and is dissected by typical CO_2 related collapse and sublimation features, similar to the features observed on the southeastern flank.

8.4.2. Seasonal Observations

The MOC-NA scenes for location A were taken during early southern summer at L_S = 297° (M12/00730 and E11/03905) and around mid-spring at L_S = 204° (M07/02129). MOC-NA scene M04/03749 covers the location a bit earlier at L_S = 195°, but no substantial difference to the M07/02129-scene has been found (figure 8.8). Additionally, three images (M12/02337, E12/00629 and R11/04160) for the mid-summer season at $L_S \approx 305°$ have been taken a few kilometres to the northeast at location B (figure 8.5). We will discuss our seasonal observations with the help of these sets of images starting at early spring (figure 8.8).
Based upon spring-time observations at L_S = 204° (figure 8.3a) as well as TES derived temperature data of that time, the sublimation temperature of CO_2 has been reached and the seasonal ice cap (figure 8.6a,d) is receding but has not yet reached its minimum extent. The polar-trough infill is characterized by CO_2-ice deposits with an overall rough surface texture that appears to be draped over the rough and undulating topography. As the topography of the trough interior is still clearly visible, we can assume that the deposit is quite thin and homogeneously spread over the surface. The transition from the southeastern 'swiss-cheese' terrain towards the southeastern wall of the trough is clearly defined by an abrupt termination of the characteristic sublimation pattern and a sudden increase in brightness, due to the illumination conditions. The transition from the trough center to the southeast-facing wall is characterized by an abrupt

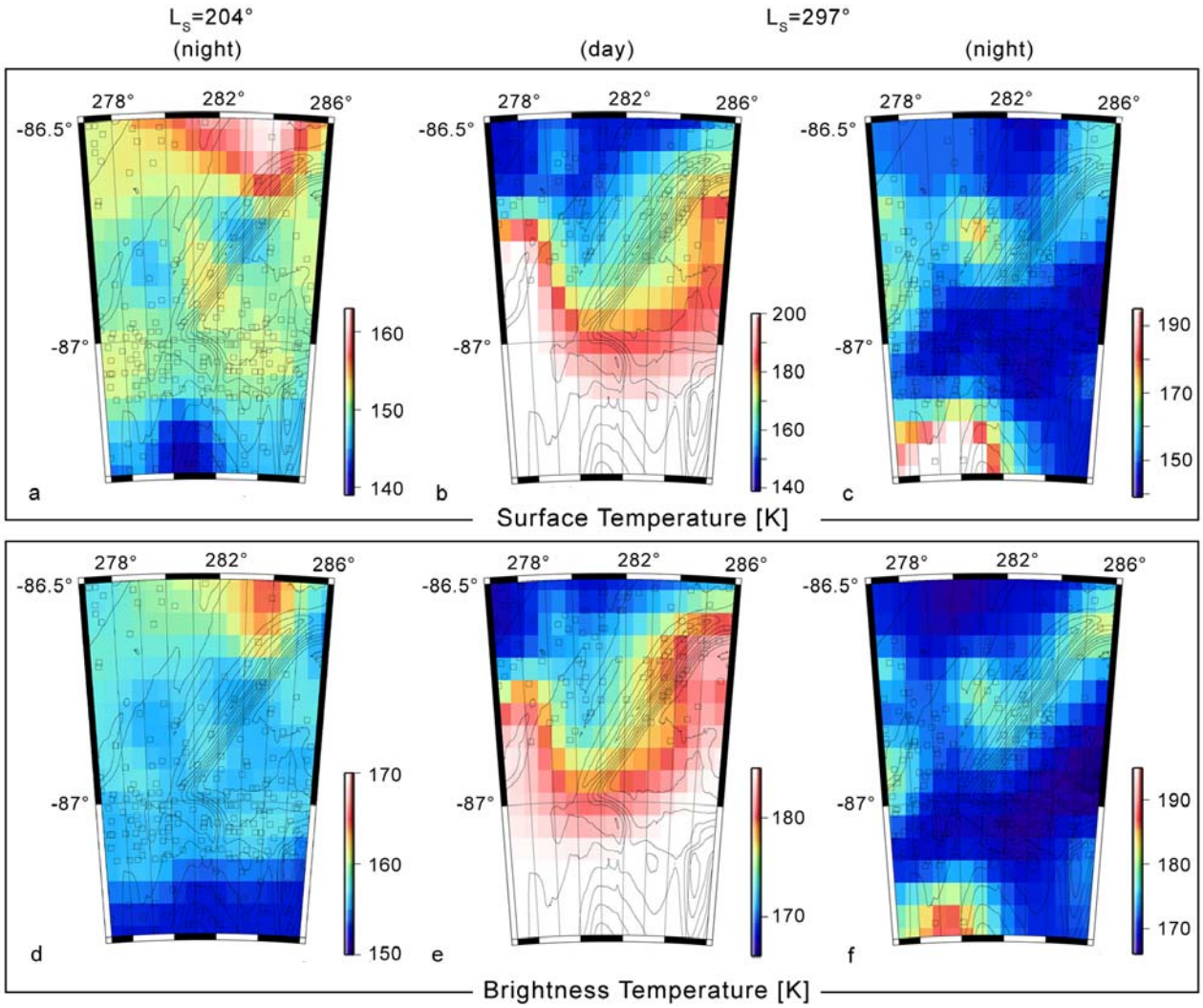

Figure 8.6.: Characterization of Martian south polar environment in terms of surface temperature and brightness temperature as obtained and derived from the Thermal Emission Spectrometer onboard Mars Global Surveyor. Seasons of interest are those during image acquisition (L_S = 204° and L_S = 297°). Contour lines represent MOLA topography, contour interval is 50 meters. Black rectangles represent individual TES data points. Note, the trough is well displayed in the brightness temperature plots.

decrease in relative brightness caused by the low sun elevation (incidence angle of 81°). The northwestern wall presents a distinct pattern of elongated grooves parallel to the main trough axis (figure 8.3a). This pattern disappears gradually towards the upper part of the wall.

In the MOC scene M09/04839 which was taken in late spring at L_S = 246° (figure 8.10), a very faint polygon pattern seems to shine through a thin CO_2 cover. Obviously, the CO_2 cover started to sublimate substantially between L_S = 204° and L_S = 246° which caused thinning of the CO_2 surface layer. This observation is in general accordance with the spring- and summertime TES derived temperature increases of up to 10 K (figure 8.6a-c).

In the early-summer image data M12/00730 and E11/03905 ($L_S \approx 297°$ of 2000 and 2001) of location A (figure 8.3b, c), several dark polygonal shapes that are covered by a thin veneer of CO_2-ice or snow become faintly visible. At the southeastern wall of the SPT,

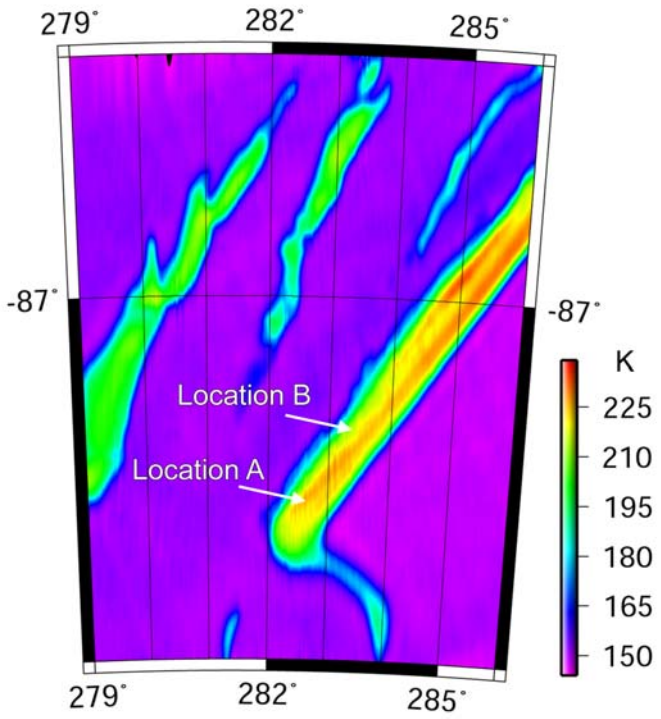

Figure 8.7: Brightness temperature (BTR) of the SPT discussed in the text on the basis of THEMIS image I08814007BTR located at -87.0° N and 253.9 ° E. Solar longitude during imaging of the THEMIS instrument is slightly later (L_S =313°) than our observations in the MOC-NA summer image data (L_S =297°). No IAU conversion during processing has been applied as the characteristic hook-shaped south-eastern trough can be localized visually well enough.

these polygons are very well defined in both summertime images. The southeastern rim of the polar trough is somewhat irregular, but still distinct in both images due to a decrease in relative brightness. The polygonal pattern, however, has changed significantly in both images (figure 8.3b, c and figure 8.11b-d). Towards the trough's center, irregular elongated patches of the underlying dark material become visible. The center is almost completely free of seasonal CO_2 and large areas of the dark material are visible. Towards the northwest, the frost cover once again becomes more dense while polygonal patterns re-appear and gradually vanish under the smooth CO_2 cover at the northern wall.

It is noteworthy that the northwestern wall of the SPT shows several fissures and furrows parallel to the main polar trough (figure 8.11a). These features have also been observed in the spring-time image and form a somewhat elongated trough-parallel pattern of rills and furrows. Since the appearance of these trough-parallel patterns is completely different from the center-trough polygons, we can assume that there is no genetic connection between these types. The distribution and geometry of these furrows, however, are exactly the same in all three images, giving an additional guarantee that the differences of polygonal patterns in the trough's center are not caused by obscured imaging characteristics. We assume that these northwestern-wall furrows could be attributed to a very slow slope-movement or that they are a surface expression of subsurface compaction of the CO_2 cover.

In mid-summer at L_S = 306° the trough in location B is completely free of seasonal CO_2 cover (figure 8.4a) and, except for very few areas at the rim of the trough where the seasonal cracked surface layer is present (figure 8.4c-e), no polygonal pattern can be observed. The sequence in figure 8.4c-e shows the region on the southeastern flank over three years.

8.4.3. Characterization of Polygonal Pattern

On a regional (kilometer) scale, the observed polygonal patterns are equally distributed in both summertime images at locations A and B (figure 8.3b-c, and figure 8.12a-b). They can be observed across the SPT surface where at least a thin cover of CO_2 still blankets

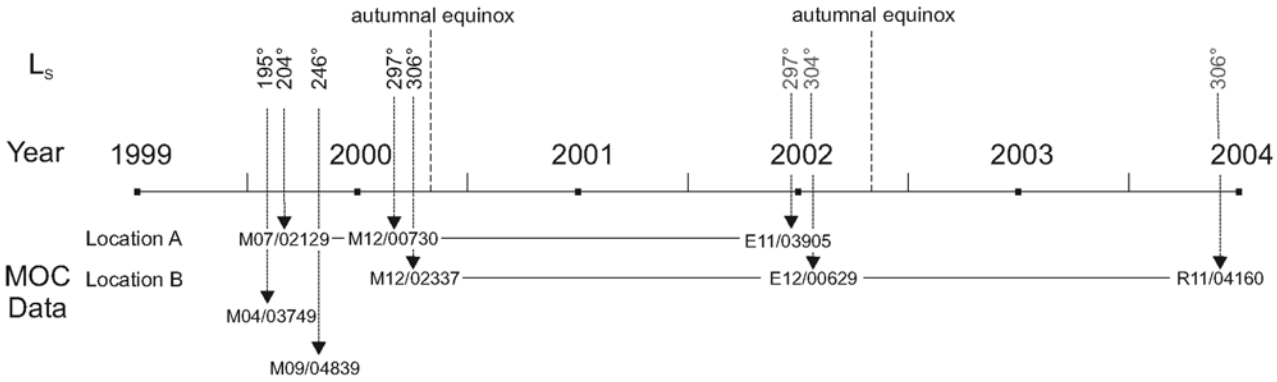

Figure 8.8.: Years and Seasons of image acquisition of the MOC images discussed in the text. MOC-image numbers located on the same level show repeated imaging of an area.

the dark-lane material. On a local (meter) scale, however, the fissure network, although showing identical shape characteristics, differs considerably in terms of the location of individual fissures (figure 8.4c-e and figure 8.11b-d).

The diameters of the individual polygons range from ≤10 meters to about 140 meters with a distinct average at diameters between 50-60 meters (12% of all diameters measured) (figure 8.12e). The slight shift in the distribution towards larger values is probably caused by a deficit in detected polygons in the small-diameter range due to limitations in image resolution. The frequency-distributions for the diameters in both summer-time images of location A are nearly identical. The size distribution fits well into the overall size-distribution measured at the south polar area (*van Gasselt et al.*, 2003b) and compares closely to that described by *Lucchitta* (1984), *Seibert and Kargel* (2001) who find similar diameter ranges between 10 to 250 meters with an average diameter of approximately 50 meters, and to that described by *Kuzmin and Zabalueva* (2003) in their analyses of 400 mid-latitude MOC-NA images. However, the mean diameter size is somewhat larger than described by *Paepe et al.* (2001) for orthogonal networks in mid-latitudes (30 meters) and by *Yoshikawa* (2000) (20 meters), who compared a few mid-latitude polygonal crack patterns with terrestrial Arctic and Antarctic polygons. Even more importantly, the values are comparable to those measured in terrestrial environments as described by e.g. *Lachenbruch* (1962); *Yershov* (2004); *Washburn* (1979a), suggesting similar cracking conditions.

The frequency-distribution of conjunction-types and conjunction-angles (figure 8.12c-d) are descriptive parameters that allow insight into the formation of polygonal crack patterns. In a simplified view, the intersection angle at a 3-ray conjunction, i.e., a conjunction between at least two polygonal troughs is generally 120°, forming a pattern of hexagonal polygon shapes. A four-ray conjunction is most likely formed when two individual polygonal fissures intersect orthogonally. A group of orthogonally intersecting polygonal fissures forms a surface characterized by an orthogonal pattern. Our data show an almost identical relative frequency of 3-ray conjunctions (65-70%) and 4- ray (30-35%) conjunctions in both images (figure 8.12d).

The conjunction angles between individual polygonal troughs range from 80° to 140° in both summer-time images with two distinct maxima at 90° to 100° (orthogonal conjunction) and at about 120° (hexagonal conjunction) (figure 8.12c). In the M12/00730-image measurements, the 90°-maximum is more distinct and contains approximately 75% of all observed conjunctions. The values for the measurements in the E11/03905-image show a distinct bimodal distribution, again with an absolute maximum at orthog-

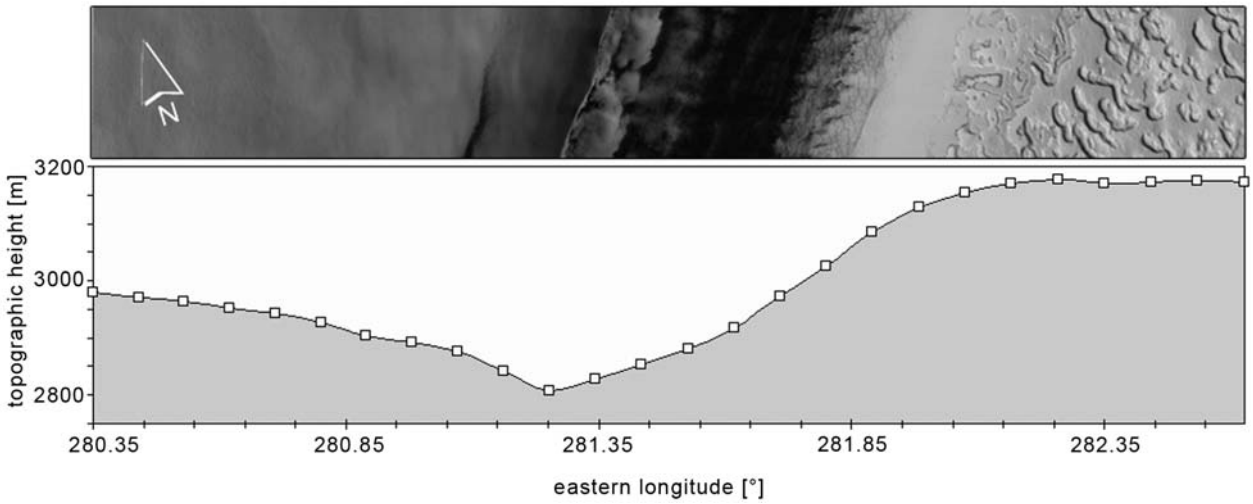

Figure 8.9.: Topographic profile as obtained by the Mars Orbiter Laser Altimeter for MOC-NA image M12/00730. The polygonal crack pattern is predominantely distributed on the southeastern and sun-lit flank below 3050 metres. The cross-section of the trough is highly asymmetrical with a steeper slope angle of about 4°-5° on the sun-lit flank and a more gentle slope angle of about 3° at the northwestern wall.

onal conjunctions. It has to be kept in mind that not all polygon fissures might have been accounted for in the statistics, due to the CO_2-cover at the polar trough boundaries and the large areas with outcrops of dark material.

The majority of polygonal troughs observed in the MOC images are slightly arcuate and extend over distances of a few hundred meters to several kilometers. A width range of two to three meters for individual polygon cracks was determined by measuring the width of the dark crack-infill. This value might be far too large and may be caused by the image-resolution limits and the diffuse distribution of dark material. The dark infill seems to be of the same composition as the dark outcrops. This suggests the polygon fissures are a trap for this material, which might be transported by seasonal polar eolian processes. This material may originate from dust that was originally incorporated into the seasonal CO_2 cover and was subsequently deposited after the CO_2 sublimated.

Despite limits of image resolution, it is clear that the polygonal fissures are not characterized by a significant central depression or upturned edges. The polygons delineated by the fissures are neither low- nor high-center polygons and the polygonal shapes appear absolutely flat (figure 8.11b-d).

8.5. Discussion and Implications

The SPT development, as observed in the MOC images and TES data, is characterised by (a) a homogeneous coverage of CO_2 in the SPT up to at least early spring (L_S = 204°) with no visible polygonal crack pattern on the surface; (b) a continuous but thin coverage of CO_2 during mid spring (L_S = 245°) where a polygonal pattern becomes faintly visible underneath the remaining CO_2 cover; (c) a well-defined polygonal crack pattern between mid-spring and early summer (L_S = 297°) when substantial amounts of seasonal CO_2 have almost completely sublimated and the remaining CO_2 coverage is distributed in a patchy way; (d) a central SPT unit that is completely free of CO_2-ice by mid-summer (L_S = 306°).

The observation that the polygonal shapes are covered during spring and become visible in summer suggests that the sequence of layers in the SPT is characterized by at least three units. The top layer is a seasonal CO_2-ice or snow layer that is present in the spring, but

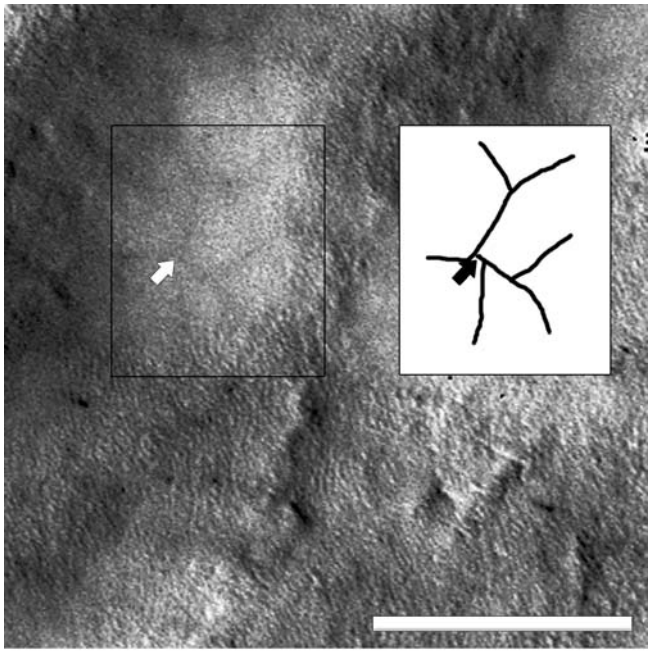

Figure 8.10: Scene of the central SPT as imaged in MOC M09/04839 taken during late spring-time. The scene shows a faintly visible polygonal pattern underneath the seasonal CO_2 cover. The scale-bar is 200 meters. North is up.

also appears to exist in the fall and winter. The middle unit, hereby referred to as the 'cracked surface layer' or intermediate unit, becomes exposed at the latest by early summer and vanishes by mid-summer. Within this layer polygonal fractures are visible. The bottom unit consists of dark material of the trough deposits (dark trough unit).

The polygonal shapes are relatively smooth and characteristics, such as upturned trough-edges and central troughs, are missing. Although the mechanism of upturning of the surface layer over an ice-wedge remains debated (e.g., *Mackay* (1980)), one common argument is that upturned rims over a fissure can be connected with the growth of ice- or sand-wedges and upturning occurs as a result of re-expansion during several freeze-thaw cycles (*Lachenbruch*, 1962). The smooth nature of the polygons, coupled with the observation that the polygonal crack patterns disappear during mid-summer, suggest ice-wedges are not formed and these cracks are (a) seasonal and (b) are recurring surface expressions of thermal contraction processes.

The types of intersections, i.e., orthogonal or hexagonal, have been discussed by various authors. Orthogonal polygon networks are most likely formed in inhomogeneous materials (*Lachenbruch*, 1962; *French*, 1996) and attributed to differences in horizontal stress, caused by horizontal temperature variations (*Lachenbruch*, 1962). This type of polygon pattern occurs where earlier cracks, which tend to follow random sinuous courses, are intersected by later fractures (*Lachenbruch*, 1962; *French*, 1996). This suggests, that the long sinuous cracks predate the perpendicular and the fractures that make up the orthogonal polygons are caused by a single cracking event. Another explanation for the irregular orthogonal pattern might be the degree of development as discussed in *Lachenbruch* (1966) and *Sletten et al.* (2003). In their work, irregular orthogonal systems are an expression of an initial cracking phase. During further development, patterned ground matures and the polygons become smaller and more regular.

Several fracture systems seem to be oriented orthogonally at the SPT (figure 8.11b). As this orientation of orthogonal fissures occurs in the vicinity of outcrops of dark sediment, it seems likely that this underlying dark material has a major influence on the horizontal temperature gradient and therefore causes a concentric fracture pattern around these dark-material patches. Subsequently, fractures form at right angles to the concentric fractures, resulting in a characteristic pattern of concentric and radial fractures.

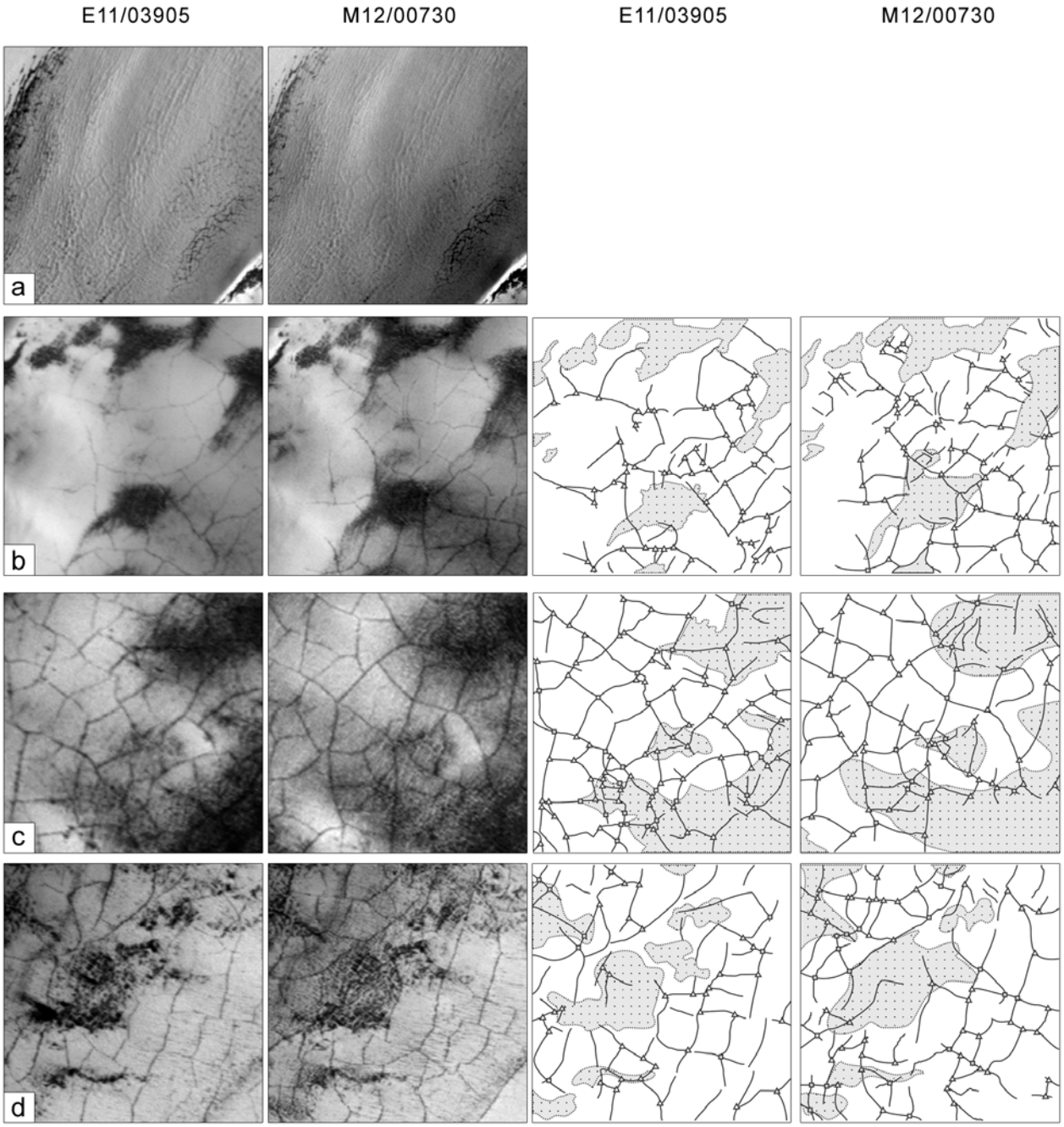

Figure 8.11.: Comparison of high-resolution scenes taken from summer-time MOC-NA images M12/00730 and E11/03905. Lower-case letters in the scenes refer to locations marked in figure 3. (a) Trough-parallel lineations on northwestern wall which can be observed in the spring- as well as in the summer-time images, image width is 6 km. (b) Northwestern part of trough, remnants of seasonal CO_2 ice cover the lower-elevation areas. Higher elevated areas are defined by characteristic dark outcrops of the trough infill underneath. Oriented orthogonal polygon pattern occur at the southern outcrop. Image width is 4 km. (c) Highly modified polygonal pattern at the trough center, image width is 3.1 km. (d) South-eastern rim near the transition to a thick CO_2 layer. The dark patches have a fine-scaled checkerboard texture. Image width is to 4.4 km. North-direction is always up.

Along with differences in the thermal property of materials, the mineralogic composition of a material can also affect the orientation in orthogonal systems (*Black*, 1952). As the material composition (*Lachenbruch*, 1962) and the temperature fluctuations (*Dostovalov and Popov*, 1966) are not precisely known, only a qualitative discussion of polygon sizes is possible here. Nonetheless, the observations are qualitatively consistent with theoretically derived predictons for crack-formation.

In order to estimate whether the composition of the cracked surface is remnant CO_2 or more likely a water- or CO_2-dust material that is distinct from the uppermost CO_2 layer, we applied a technique, devised by *MacKay* (1986) at Illsarvik, to determine the linear expansion coefficient. *MacKay* (1986) made use of theoretical models by e.g. *Lachenbruch* (1962) to estimate the coefficient of linear expansion α [1/°C] which controls cracking of surface material. To estimate the 'apparent' coefficient of linear expansion α, the crack width (ΔL), the distance between two parallel cracks on the surface L and the mean ground temperature (T) have been used:

$$\alpha = \frac{\sum \Delta L}{L \cdot \Delta T} \tag{8.1}$$

where Δ T is the temperature change relative to 273 K (*MacKay*, 1986).

In order to estimate α, we have to consider that an individual fissure width can only be approximated. Due to the limits of image resolution, the one to two meter widths must be viewed as an absolute maximum and are most likely overestimates. Surface temperatures for the time period of cracking (i.e., winter) are not provided by TES. While 150 K might be a bit warmer than the mean winter temperature at the location of study, this value was used to compare it with the fit provided by *Mellon* (1997). We measured across three parallel fissures at two locations:

Location 1: L=125 meters, $\sum \Delta$L=3 m to 6 m, ΔT=150 K, and Location 2: L=180 meters, $\sum \Delta$L=3 m to 6 m, ΔT=150 K.

We obtained rough estimates for α that range from $160 \cdot 10^{-6}$/K to $320 \cdot 10^{-6}$/K for location 1 and $110 \cdot 10^{-6}$/K to $220 \cdot 10^{-6}$/K for location 2.

The coefficient of linear expansion for water-ice has been measured to range from $45 - 50 \cdot 10^{-6}$/°C for temperatures between 0° to -40°C; this range applies to terrestrial thermal contraction cracking (*MacKay*, 1986; *Lachenbruch*, 1962). *French* (1996) provides the slightly lower value of $17 \cdot 10^{-6}$/°C. On Mars, a fit function of $2.47 \cdot 10^{-7}$T-$1.17 \cdot 10^{-5}$K, which is valid in a temperature range from below 150 K to 273 K, has been derived by *Mellon* (1997). These estimates are all based on experiments by *Hobbs* (1974). Although our values are one order larger than those provided by *Mellon* (1997) for Martian conditions at these temperatures, they remain in the range of laboratory experiments for water-ice ($\alpha = 350 \cdot 10^{-6}$/°C) and measurements at Illisarvik ($\alpha = 50 - 400 \cdot 10^{-6}$/°C), as described in *MacKay* (1986). However, in the case of water ice with considerable admixtures of dust or fine grained material the linear expansion would be significantly lower (*Mellon*, 1997).

These estimates and the fact that thermal contraction fissures occur in a thin layer only, suggest that the intermediate cracked surface unit may consist of water-ice that is seasonally overlain by CO_2 ice.

The thickness of the cracked layer can not be determined from image observations. However, we suggest that the cracked surface layer is probably thinner than the overlying CO_2 ice-cover, which is known to be in range of a few centimeters to decimeters (*Smith et al.*, 2001; *Aharonson et al.*, 2003). This assumption is based upon the observation that the cracked surface is exposed in early summer and completely removed by mid-summer, whereas the removal of centimeters to decimeters of more volatile CO_2 takes from early spring to mid- summer.

8.6. Model for Polygon Formation

While the structure of both Martian polygons and their terrestrial counterparts are similar, the timeframe for formation and the structure of individual surface units are different. Based upon our observations and discussions, we create a model to reconstruct the seasonal development of polygonal cracks figure 8.13.

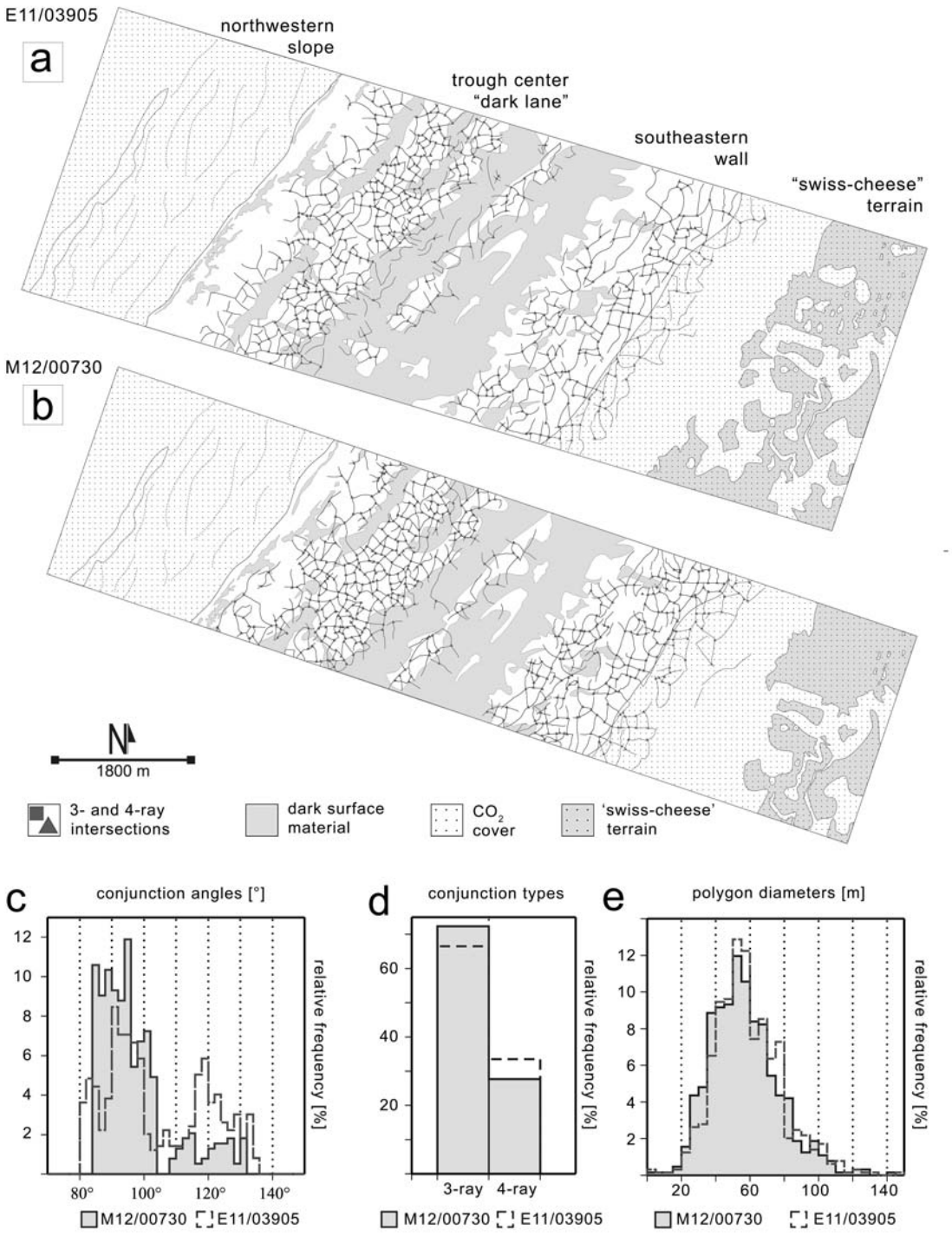

Figure 8.12.: Sketch maps of surface features and polygonal crack patterns in MOC-NA M12/00730 (a) and E11/03905 (b) scenes of location A. North is up. Below: Polygon statistics for conjunction angles (c), conjunction types (d), and diameters (e).

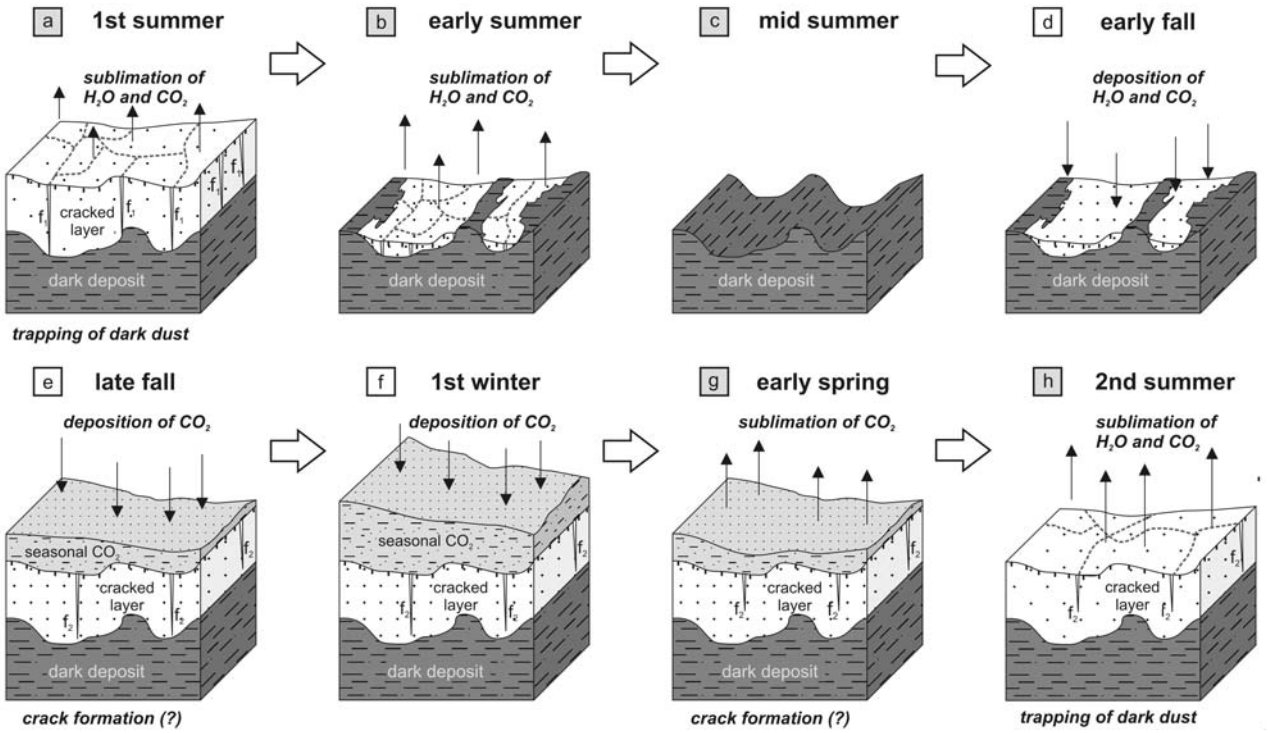

Figure 8.13.: Three-layer-model for seasonal changes in the SPT during one Martian year starting in summer. Top layer is seasonal CO_2 snow and -ice with a thickness of several centimeters (*Smith et al.*, 2001; *Aharonson et al.*, 2003). The second layer represents a thin veneer of cracked material which might be H_2O ice. The third (bottom) layer is the SPT infill of dark material. Thicknesses of individual layers are highly exaggerated for display purposes. Gray boxes with letters represent scenarios which are covered by image observations. The time and time-span for formation of contraction cracks is uncertain. The letters f_1 and f_2 are first-generation and second-generation fissures, respectively. For a detailed descriptionsee main text.

In early summer (location A: M12/00730 and E11/03905 at L_S = 297°), seasonal CO_2 blankets the polar trough rims. Most of the CO_2 inside the SPT sublimated, revealing a thin veneer of what is probably less volatile H_2O-ice. This veneer shows a characteristic polygonal crack network. Where the cracked surface layer has been removed through sublimation the dark underlying trough infill can be observed (figure 8.13a-b).

In mid-summer (location B: M12/02337, E12/00629, and R11/04160 at L_S = 306°), the central SPT surface is free of the cracked surface layer and only the dark trough infill is exposed (figure 8.13c). Large temperature values derived from the TES data support this observation.

Presumably during early fall, first a thin layer of H_2O then CO_2 is deposited on the trough surface (figure 8.13d-e). If temperature gradients are large enough, the first thermal contraction cracks could then form in late fall. If the overlying CO_2-layer insulates the H_2O-layer, thermal contraction cracking might occur even during early spring, as observed on Earth (*Lachenbruch*, 1962). In this case, CO_2 insulates underlying layers in a similar fashion as the so-called 'active layer' on Earth (figure 8.13g).

In early spring of the following year (location A: M04/03749 at L_S = 195° and M07/02129 at L_S = 204°), the trough is covered by a thick veneer of CO_2 frost. No characteristic polygon patterns can be detected.

During mid spring (location A: M09/04839 at L_S =

246°), CO_2 is sublimating and a diffuse polygonal pattern can be seen through the CO_2 cover. If the insulating effect of the CO_2 diminishes, thermal gradients might become large enough to cause thermal stresses that exceed the strength of the surface material. The dust, which is incorporated into the sublimating CO_2 layer, is now redistributed on the H_2O layer and fills the polygonal troughs the following summer (figure 8.13h).
This sequence is in general agreement with observations made in periglacial environments on Earth (e.g., *Lachenbruch* (1962)).

8.7. Conclusions

The discovery and reconstruction of active surface cracking at the south pole yield several important conclusions:
1. Based upon three years of observation in high-resolution MOC image data, polygonal patterns change annually in regions where conditions are favourable, i.e. temperature gradients cause cracking of a nintermediate layer which sublimates and deposits annually. So far, we have not found any evidence for changing crack patterns in other locations than the SPT discussed herein.
2. We see that geologic processes are very active on Mars, which shows that the south polar cap (and its neighbouring units) must be considered as an individual geologically active unit (*Thomas et al.*, 2000).
3. We found strong indications that a layer of H_2O underlies the seasonal CO_2 frost cover. This layer cracks due to thermal contraction and sublimates during summer. This intermediate layer plays a significant role in the development (i.e., shape and size) of thermal contraction cracks.
4. The shape and scale of polygonal networks in the south polar trough compares closely to terrestrial permafrost polygons.
5. The shape and scale of polygonal patterns are influenced by the compositional and thermal properties of the dark trough infill. Randomly and orthogonally oriented patterns on Mars are similar to those observed in terrestrial environments; presumably, similar parameters influence the patterns in both environments.
6. At this SPT, ice-wedging can be ruled out, since (a) the cracked intermediate layer is not stable throughout a Martian year and (b) characteristic upturned edges at fissures are missing.
7. Each year, dark sedimentary material in the SPT accumulates after the cracked surface layer disappears and the fissure infill remains. The amount of sediment that accumulates each year is unknown.
8. In this context, climatic change plays no role in the evolution of polygonal cracks, since this process is repeated every year and subject to the annual global CO_2/H_2O cycle.
9. The appearance of the polygonal pattern (shape, size and morphology) could be used to identify similar terrain on Mars in order to locate possible sub-CO_2 water ice and distinguish units of ice-wedging and fissuring.
However, the thermal environment and mechanical properties of the surface material were not incorporated into this model of the cracking process. This task will be handed over to those with expertise in this field. In order to fully understand these processes in the south polar region, this type of research must be undertaken. Greater knowledge of these directly observable processes will aid in understanding the behaviour and development of thermal contraction cracking as well as possible subsequent wedging in mid-latitudes.

Acknowledgements

We wish to thank Malin Space Science Systems, the MOLA Science Team, and the TES and THEMIS teams at Arizona State University for providing the images and data to the public. We would like to thank the anonymous reviewers who helped to improve the manuscript by their comments and remarks.

8.8. Unpublished Supplement

The south-polar distribution of polygons has been mapped and was published in extended conference

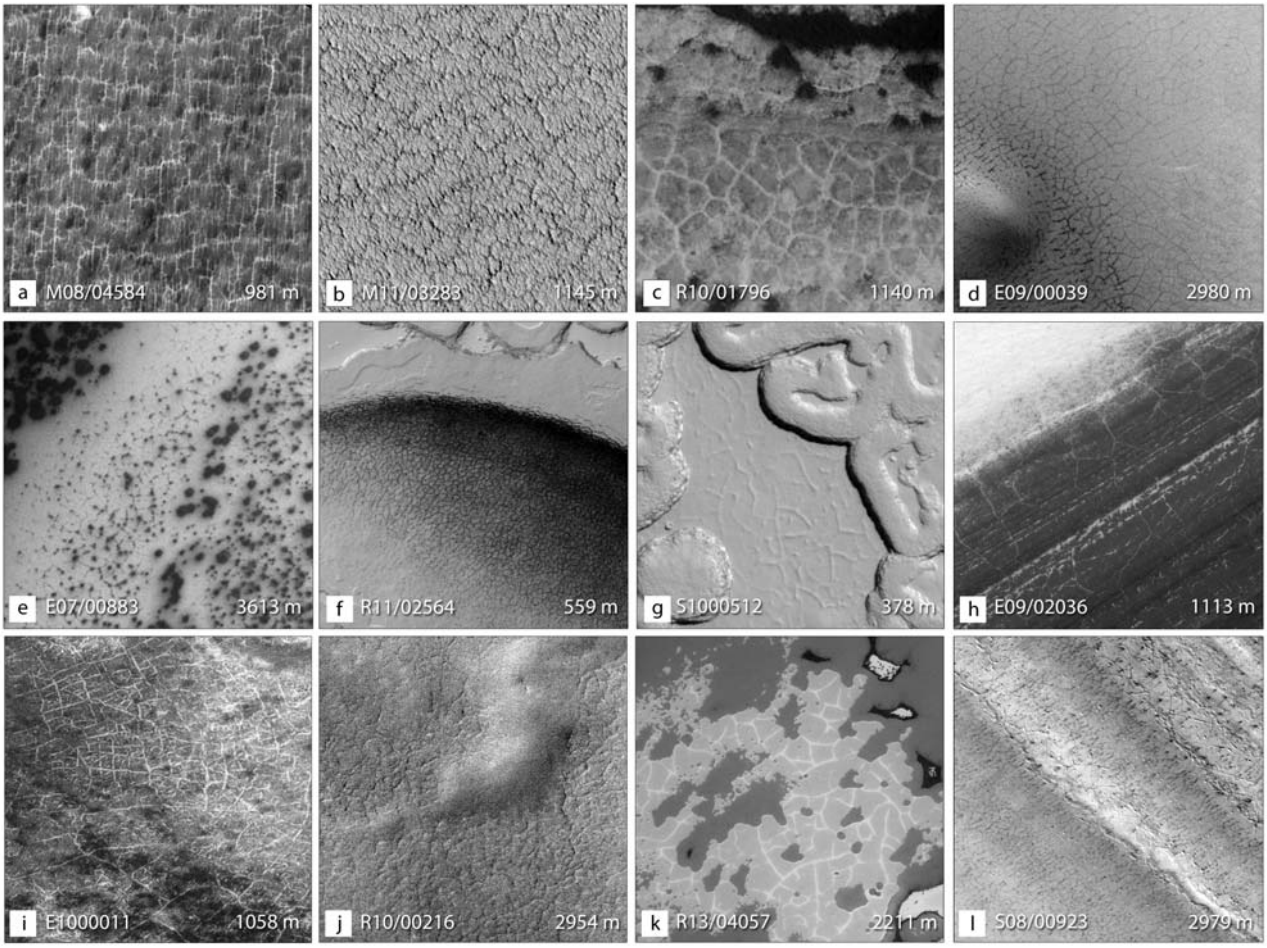

Figure 8.14.: Examples of mapped and categorized polygonal patterns at the south-polar region at latitudes south of 75°S and plotted in figure 8.15; for image scales see MOC-NA scenes, scales refer to image extent. [a-b] plains-type polygons, [c] hexagonal polygon types, [d-e] degenerated polygon type, [f] depression-wall polygons, [g] swiss-cheese types (see text), [h] polar trough-related polygons, [i] complex polygons, [j] wrinkled polygons, [k] plains-type polygons in thin defrosting CO_2 layer, [l] extension cracks (see text).

abstracts (*van Gasselt et al.*, 2003b; *van Gasselt et al.*, 2004). Recent mapping work includes all MOC releases (S10) provided to the public in 2006. Interpretation of distribution aspects, morphologies, and variations within a seasonal context as well as under consideration of TES-derived temperature and surface pressure data is still preliminary and needs further work. With the unfortunate termination of the Mars Global Surveyor mission, images of the Mars Orbiter Camera data will not be obtained anymore and, consequently, all MOC images acquired thus far will be released to the public in 2007. The final releases will be added to this distribution and will complete the current search for polygonal features in the south polar area. Up to now, approximately 78,000 MOC-NA images have been obtained from Mars since 1999; with the S10 release of MOC, 12,150 images cover the south polar area south of 75°S. These MOC scenes have been thoroughly studied and a number of 1,600 images showing polygonal features in different shapes and sizes could be extracted. The polar-polygon distribution is shown in figure 8.15, various morphological types are shown and described in figure 8.14. Polygonal patterns do often occur in the south po-

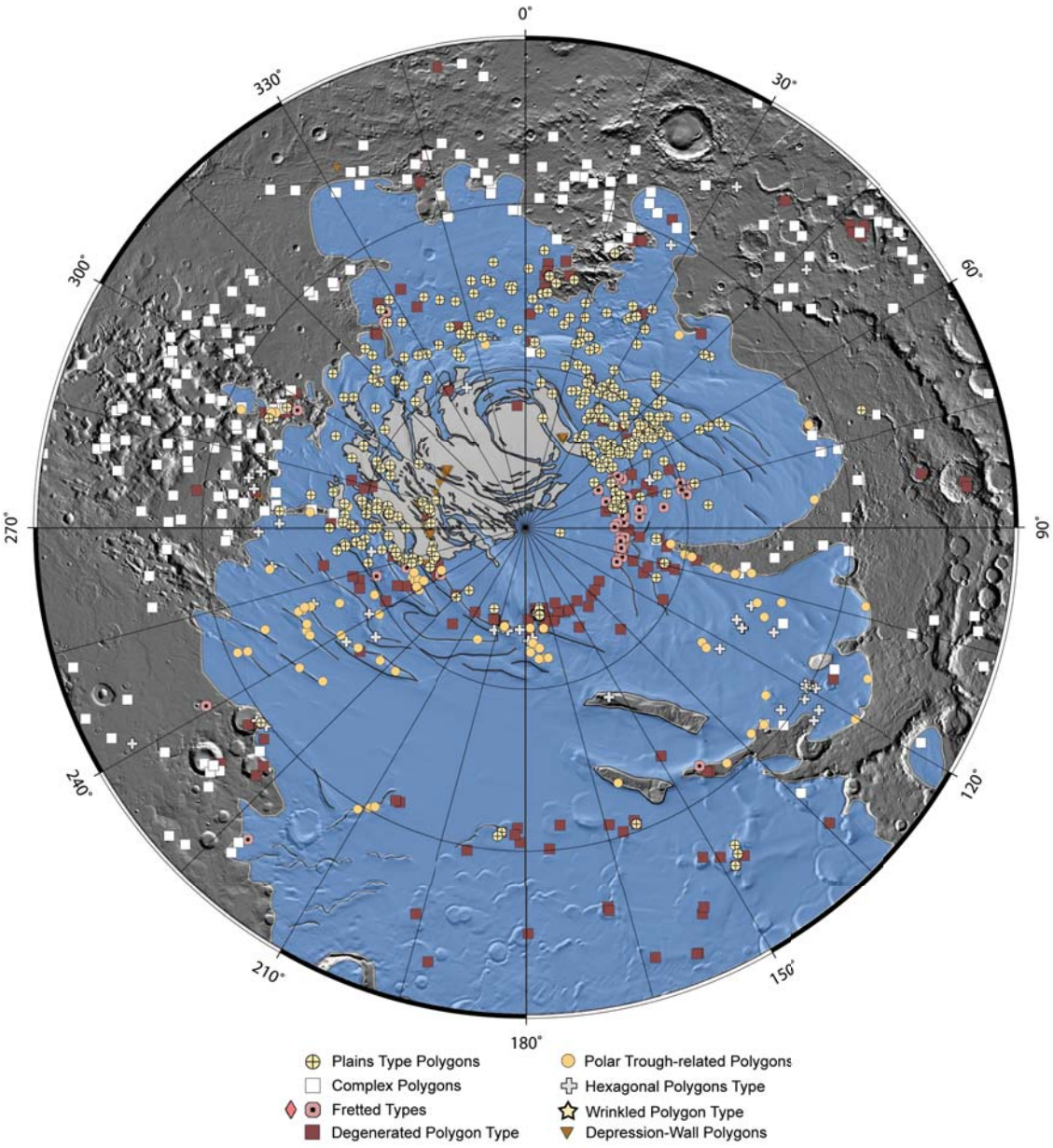

Figure 8.15.: Stereographic projection of the south polar cap south of 75°S with all occurrences of polygonal features that were categorized. Classes shown in the legend are displayed in figure 8.14; see clear latitudinal distribution of e.g., depression-wall polygons, fretted-type polygons and complex polygons; background data is MOLA shaded relief, blue area marks the extent of the South Polar Layered Deposits (SPLD), white area is the residual ice cap, unpublished work, see also *van Gasselt et al.* (2003b); *van Gasselt et al.* (2004).

lar area, especially in connection with the residual cap; not all of these features are considered to be connected to thermal contraction processes but to (a) settling of material at trough walls (see discussion and examples in main paper), (b) seasonal deposition and sublimation cycles of CO_2 within the 'swiss-cheese' terrain (figure 8.14g), or to (c) extensional stresses (figure 8.14l). Several polygon types are restricted to small confined areas only or their occurrences show a distinct latitudinal dependence. Complex polygons (figure 8.14i) occur in seasonal CO_2 deposits outside of the polar layered deposits only, their type loca-

tion is the Cavi Angusti area (270°E). Depression-wall polygons (figure 8.14f) only occur at south polar troughs near the south pole and are restricted to the area around 270°E and south of 85°S. Fretted-type polygons (figure 8.14i) occur almost exclusively at the head of the Chasma Australe near the pole (90°E). Other types occur exclusively on the polar layered deposits (plains-type polygons, degenerated-type polygons) and are connected to circum-polar troughs (polar-trough polygons, figure 8.14h).

Note:

This paper has been published in a slightly modified version in Journal of Geophysical Research referenced as van Gasselt, S., D. Reiss, A. K. Thorpe, G. Neukum (2005): Seasonal variations of polygonal thermal contraction crack patterns in a south polar trough, Mars, *J. Geophys. Res.*, **110**(E9): E098002, doi: 10.1029/2004JE002385. □